| | |
|---|---|
| **Preprint Title** | Vibration analysis and pull-in instability behavior in multi walled piezoelectric nano-sensor with fluid flow conveyance: influences of surface/interface energy |
| **Authors** | Sayyid H. Hashemi Kachapi |
| **Publication Date** | 17 Dez 2019 |
| **Article Type** | Full Research Paper |
| **Supporting Information File 1** | Supporting Information.zip; 176.5 KB |
| **ORCID® iDs** | Sayyid H. Hashemi Kachapi - https://orcid.org/0000-0002-5384-9724 |

# Vibration analysis and pull-in instability behavior in multi walled piezoelectric nano-sensor with fluid flow conveyance: influences of surface/interface energy

**Sayyid H. Hashemi Kachapi**[1]

[*] Department of Mechanical Engineering, Babol Noshirvani University of Technology, P.O.Box484, Shariati Street, Babol, Mazandaran47148-71167, Iran

**Abstract**

In this work, surface/interface effects for pull-in voltage and viscous fluid velocity effects on dimensionless natural frequency (DNF) of fluid-conveying multi walled piezoelectric nanoresonator (FC-MWPENS) based on cylindrical nanoshell is investigated using the Gurtin–Murdoch surface/interface theory. The nano-sensor is embedded in viscoelastic foundation, nonlinear van der Waals and electrostatic forces. Hamilton's principle is used for deriving of the governing equations and boundary conditions and also the assumed mode method is used for changing the partial differential equations into ordinary differential equation. The influences of the surface/interface effect such as Lame's constants ($\lambda^{I,S}, \mu^{I,S}$), residual stress ($\tau_0^{I,S}$), piezoelectric constants ($e_{31p}^{s_k}, e_{32p}^{s_k}$) and mass density ($\rho^{I,S}$) are considered for analysis of dimensionless natural frequency respect to viscous fluid velocity $\bar{u}_f$ and pull-in voltage $\bar{V}_{DC}$ of FC-MWPENS.

**Keywords:** fluid-conveying multi walled piezoelectric nano-sensor; surface/interface effect; pull-in voltage; stability analysis; viscous fluid velocity; electrostatic excitation; van der Waals force.

**Nomenclature**: Notation and symbols

| symbols | Description | symbol | Description |
|---|---|---|---|
| $h_{Nn}$ | Thickness of nanoshell (NS) | $h_{pn}$ | Piezoelectric layer thickness |
| $L$ | piezoelectric nanoshell Length | $E_{pn}$ | Young modulus of piezoelectric layer |
| $R_n$ | The mid-surface radius | $\upsilon_{pn}$ | Poisson ratio of piezoelectric layer |
| $x$ | Axial direction | $\rho_p$ | Mass density of piezoelectric layer |
| $\theta$ | Circumferential direction | $e_{31pn}, e_3$ | Piezoelectric constants |
| $z$ | Radius direction | $\eta_{33pn}$ | Dielectric constant |
| $E_{Nn}$ | Young modulus of nanoshell | $s_{kn}$ | Piezoelectric inner and outer surface |
| $\upsilon_{Nn}$ | Poisson ratio of nanoshell | $\lambda^{s_{kn}}, \mu^{s_{kn}}$ | Lame's constants of piezoelectric layer |
| $\rho_{Nn}$ | Mass density of nanoshell | $\bar{E}_{pn}$ | Electric field |
| $I_{kn}$ | Nanoshell Inner and outer surface | $D_{zpn}$ | Electric displacement |
| $\lambda^{I_{k(n)}}, \mu^{I_{k(n}}$ | Lame's constants of nanoshell | $\tau_0^{s_{kn}}$ | Residual stress of piezoelectric layer |
| $\tau_0^{I_{k(n)}}$ | Residual stress of nanoshell | $e_{31pn}^{s_k}, e_3^{s}$ | Surface piezoelectric constants |
| $\rho^{I_{k(n)}}$ | Nanoshell interface mass density | $\rho^{s_k n}$ | Piezoelectric surface mass density |
| $C_{ijNn}$ | Elastic constant of nanoshell | $C_{ijpn}$ | Elastic constant of piezoelectric layer |
| $\sigma_{ijNn}$ | Middle stress of nanoshell | $\sigma_{ijpn}$ | Middle stress of piezoelectric layer |

[1] The corresponding author, sha.hashemi.kachapi@gmail.com

| | | | |
|---|---|---|---|
| $\kappa_{(x,\theta)}$ | Curvature components | $V_{pn}$ | Piezoelectric voltage |
| $\varepsilon^0_{(x,\theta)}$,$\gamma^0_{x\theta}$ | Middle surface strains | $\pi_n$ | Total strain energy |
| $u$ | Displacement of $x$ direction | $T_n$ | Total kinetic energy |
| $v$ | Displacement of $\theta$ direction | $I_n$ | Mass moments of inertia |
| $w$ | Displacement of $z$ direction | $C_{wn}$ | Damping coefficient |
| $\nabla$ | Laplace operator | $K_{wn}$ | Winkler modulus |
| $\omega$ | Natural frequency | $K_{pn}$ | Pasternak Shear modulus |
| $M$ | Total mass matrix | $W_n$ | Total work |
| $C$ | Total damping coefficient | $K_n$ | Total stiffness matrix |
| $\bar{F}$ | Loads by piezoelectric voltage | $b_n$ | The nano-sensor gap width |
| $V_{DnC}$ | direct electric voltage | $\bar{C}^{L}_{vdwn}$ | Linear van der Waals coefficient |
| $\bar{C}^{NL}_{vdwn}$ | Nonlinear van der Waals coefficient | | |

**1: Introduction**

Nanomechanical sensors and actuators specially combined with piezoelectric materials are widely used in modern engineering which have received considerable attention from researchers around the world, due to their unique features and widespread applications [1-3]. On the other hand, due to excessive use of nano-sensor, especially piezoelectric nano-sensor in vibration devices, modeling their mathematical modeling and vibration behaviors are essential and due to experimental observation, for the dynamics analysis and the mathematical modeling of these nano-structures, the size dependent parameters should be contained in theoretical models. For this reason, surface/interface elasticity, which was brought up by Gurtin and Murdoch, is taken into consideration [4]. Also, multi walled nanoshell (MWNS) are structurally built by multi concentric single-walled nanoshell (SWNS) and those mechanical properties are superior to the mechanical properties of SWNS. As a result, MWNSs are preferred, in some applications such as nanoresonator.

Many studies have been carried out on the vibration and stability analysis of nanostructure that some of them are reviewed here. Strozzi and Pellicano investigated vibration analysis of triple-walled carbon nanotubes (TWNTs) subjected to the interlayer van der Waals (vdW) force in the framework of the Sanders–Koiter shell theory [5]. Also, based on nonlocal cylindrical shell theory, Ghorbanpour Arani et al. studied nonlinear vibration and instability of the double walled boron nitride nanotubes [6]. Malihi et al. investigated the effect of nonzero initial conditions, nonlinear coefficient of squeeze film air damping and van derails effect on the stability of torsional nanomirrors for obtained dynamic pull-in instability voltage using the size effect [7]. Fakhrabadi et al. utilized the modified couple stress theory to investigate the effects of various fluid parameters on pull-in voltages of carbon nanotubes conveying- viscous fluid [8]. Also, vibration analysis of viscoelastic double-walled carbon nanotube (DWCNT) unified with ZnO layers and subjected to magnetic and electric fields are studied by Fereidoon et al. [9]. Recently, Hashemi Kachapi et al. presented Gurtin–Murdoch surface/interface theory to investigate linear and nonlinear vibration analysis of piezoelectric nanostructures [10-13]. Also, nonlinear buckling and postbuckling behavior of functionally graded piezoelectric cylindrical nanoshells under lateral pressure are studied by Fang et al. using surface energy effect [14]. Wang utilized surface strain gradient elasticity to study a meticulous solution to the anti-plane shear problem of a circular elastic inhomogeneity [15]. Nami et al. utilized nonlocal elasticity theory and trigonometric shear deformation theory to investigate static analysis of

rectangular nanoplates [16]. The Gurtin–Murdoch surface theory is presented by Sigaeva et al. to stydy the universal model describing plane strain bending of a multilayered sector of a cylindrical tube [17]. Karimipour et al. presented modified strain gradient theory (MSGT) and Gurtin–Murdoch surface elasticity to investigate the size dependent nonlinear pull-in instability [18]. A new size-dependent nonlinear model for the analysis of the behavior of carbon nanotube resonators is introduced by Farokhi et al. based on modified couple stress theory [19]. Surface stress effect on the vibration of cylindrical nanoshell according to the Gurtin- Murdoch theory is investigated by Rouhi et al. [20]. Liu et al. utilized a new finite element method for modeling thin structures with surface effects by using layered shell elements [21].

To the best knowledge of the author that surface/interface effect on pull-in voltage, viscous fluid velocity effects and dimensionless natural frequency of multi walled piezoelectric nano-sensor conveying viscous fluid based on cylindrical has not been studied yet. In the present study, the effect of surface/interface parameters such as Lame's constants ($\lambda^{I,S}, \mu^{I,S}$), residual stress ($\tau_0^{I,S}$), piezoelectric constants ($e_{31p}^{s_k}, e_{32p}^{s_k}$) and mass density ($\rho^{I,S}$) are studied for analysis of dimensionless natural frequency respect to viscous fluid velocity $\bar{u}_f$ and pull-in voltage $\bar{V}_{DC}$ of FC-MWPENS that subjected to direct electrostatic voltage DC with nonlinear excitation, nonlinear van der Waals force and viscoelastic foundation.

## 2: Mathematical formulation

A schematic diagram of multi walled piezoelectric nano-sensor embedded with fluid-conveying in inner layer and with two piezoelectric layers and viscoelastic foundation medium in outer layer is shown in Figure 1 (a-c). The geometrical parameters of the cylindrical shell are the length $L$, the mid-surface radius $R_n$ with nanoshell thickness $2h_{Nn}$ and coated by two piezoelectric layers with total thickness $2h_{pn}$ for the outer walled and also the mid-surface radius $R_{k+1}$ and nanoshell thickness $2h_{N(k+1)}$ for the other inner walled layers. All of the physical and geometrical properties of the mentioned nanostructures for SWPENS can be seen in work done by Hashemi Kachapi et al. in reference [11, 13].

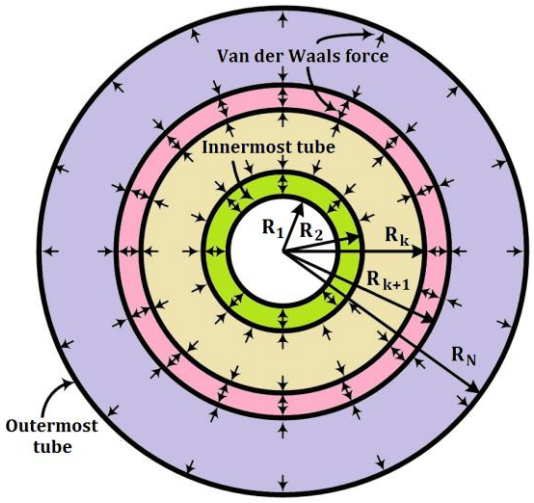


(a) Illustration of vdW forces between two adjacent tubes of a multiple shell cross section of a multi walled carbon nanotube (MWCNT)

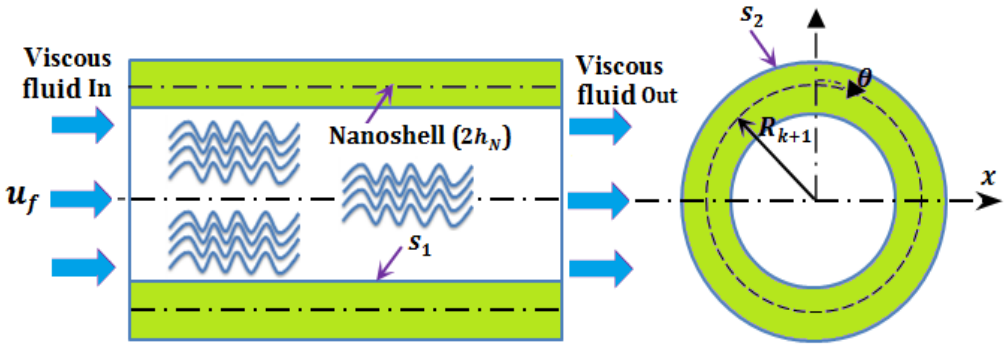


(b) Modeling of $1 \ldots k+1$ tube of MWCNT as a fluid-conveying nano-sensor with surface model

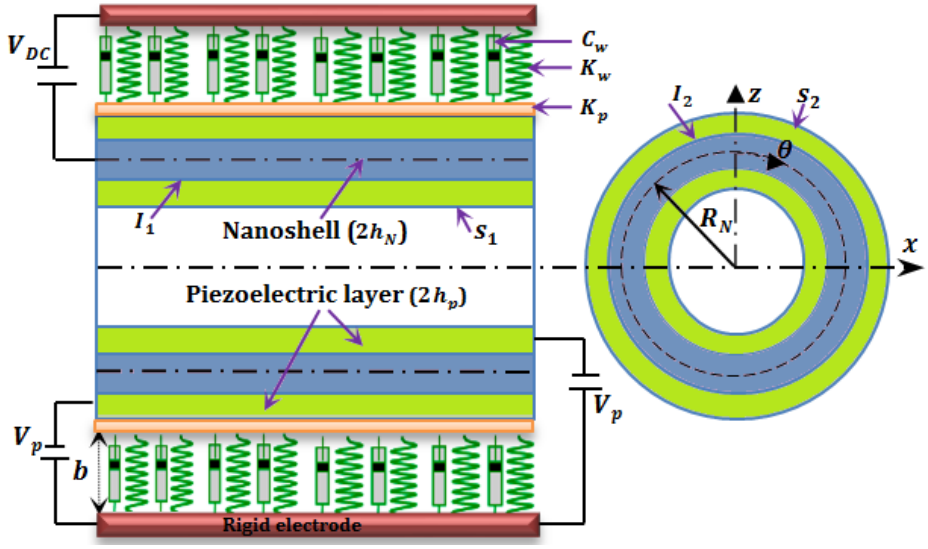


(c) Modeling of last tube of MWCNT as a piezoelectric nano-sensor with surface/interface model

**Fig. 1.** Fluid-conveying multi walled piezoelectric nano-sensor

**2-1: Non- classical Shell theory**

Within the framework of Gurtin–Murdoch surface/interface elasticity theory, the normal stresses $\sigma_{xx}$ and $\sigma_{\theta\theta}$ can be written as [4, 10-14]

$$\sigma_{xx(N,p)} = C_{11(N,p)}\varepsilon_{xx} + C_{12(N,p)}\varepsilon_{\theta\theta} - e_{31p}\bar{E}_{xp} + \frac{\upsilon_{(N,p)}\sigma_{zz(N,p)}}{1-\upsilon_{(N,p)}}, \quad (1)$$

$$\sigma_{\theta\theta(N,p)} = C_{21(N,p)}\varepsilon_{xx} + C_{22(N,p)}\varepsilon_{\theta\theta} - e_{32p}\bar{E}_{\theta p} + \frac{\upsilon_{(N,p)}\sigma_{zz(N,p)}}{1-\upsilon_{(N,p)}}, \quad (2)$$

$$\sigma_{x\theta(N,p)} = C_{66(N,p)}\gamma_{x\theta}, \quad (3)$$

Where based on nonclassical continuum model, $\sigma_{zz}$ is expressed as following

$$\sigma_{zz} = \frac{z}{h_{Nn}+h_{p2}}\left((\tau_0^{ps}+\tau_0^{NI})(\frac{\partial^2 w}{\partial x^2}+\frac{1}{R^2}\frac{\partial^2 w}{\partial \theta^2}) - (\rho^{ps}+\rho^{NI})\frac{\partial^2 w}{\partial t^2}\right), \quad (4)$$

In all following formulations, all of the piezoelectric parameters (the materials and geometrical parameters) are neglected for first layer and to be zero and all of the materials and geometrical parameters of nanoshell in the first layer are similar to the second layer of nanostructure.

Also all coefficients and phrases of Eqs. (1)- (4) such as nonlinear deflection, displacement fields and curvatures, relations of Gurtin–Murdoch surface/interface elasticity theory and etc. can be expressed in full detail in reference [11-13].

**2-2: Governing equations**

In current section, the governing equations and boundary conditions of the MW piezoelectric nanostructure are obtained by using the Hamilton principle. The total strain energy considering the surface/interface effect is written as:

$$\begin{aligned}\pi_n &= \frac{1}{2}\int_0^L\int_0^{2\pi}\int_{-h_N}^{h_N}\sigma_{ijN}\varepsilon_{ij}\,R dz d\theta dx + \frac{1}{2}\int_0^L\int_0^{2\pi}\int_{h_N}^{h_N+h_p}\left(\sigma_{ijp}\varepsilon_{ij}-\bar{E}_{zp2}D_{zp}\right)R dz d\theta dx \\ &+\frac{1}{2}\int_0^L\int_0^{2\pi}\left(\sigma_{ij}^{s_2}\varepsilon_{ij}-\bar{E}_{zp}D_i^{s_2}\right)(R+h_N+h_p)\,d\theta dx + \frac{1}{2}\int_0^L\int_0^{2\pi}\sigma_{ij}^{s_1}\varepsilon_{ij}\,(R-h_N)d\theta dx \\ &= \frac{1}{2}\int_0^L\int_0^{2\pi}\begin{Bmatrix}N_{xxn}\varepsilon_{xx}^0+N_{\theta\theta n}\varepsilon_{\theta\theta}^0+N_{x\theta n}\gamma_{x\theta}^0+M_{xxn}\kappa_{xx}+M_{\theta\theta n}\kappa_{\theta\theta}+M_{x\theta n}\kappa_{x\theta}\\ +\eta_{33}\bar{E}_{zp}^2h_p\end{Bmatrix}R_n d\theta dx\end{aligned} \quad (5)$$

In Eq. (5), the forces ($N$) and moment ($M$) resultants are defined in reference Hashemi Kachapi et al. [13] for SWPENS. And, as explained, all the sentences mentioned in reference [13] belong to the last wall (in this article, the third wall), which is considered a nanoshell with two piezoelectric layers, and in the other walls (in this article, the first and second walls) are not considered piezoelectric effects. The kinetic energy of the FC-MWPENS can be written as:

$$T_n = \frac{1}{2}\iint I_n\left(\left(\frac{\partial u_n}{\partial t}\right)^2+\left(\frac{\partial v_n}{\partial t}\right)^2+\left(\frac{\partial w_n}{\partial t}\right)^2\right)R_n d\theta dx \quad (6)$$

where

$$I_n = \int_{-h_N}^{h_N}\rho_N\,dz + \int_{-h_N-h_p}^{-h_N}\rho_p\,dz + \int_{h_N}^{h_N+h_p}\rho_p\,dz + \rho^{S,I} = 2\rho_N h_N + 2\rho_p h_p + 2\rho^{ps} + 2\rho^{NI}$$

The work done by the surrounded viscoelastic medium including the viscoelastic foundation and also the nonlinear van der Waals interaction and the nonlinear electrostatic force for example for three walled piezoelectric nano-sensor (TWPENS), respectively, can be expressed as [13, 22, 23]

$$\begin{aligned}W_{vdw} &= \int_0^L\int_0^{2\pi}\int_0^{w_1}\left(C_{vdw(12)}^{L}(w_2-w_1)+C_{vdw(12)}^{NL}(w_2-w_1)^3\right)dw_1\,R_1 d\theta dx \\ &+\int_0^L\int_0^{2\pi}\int_0^{w_2}\begin{pmatrix}C_{vdw(23)}^{L}(w_3-w_2)+C_{vdw(23)}^{NL}(w_3-w_2)^3\\ -\left(\frac{R_1}{R_2}\right)\left(C_{vdw(12)}^{L}(w_2-w_1)+C_{vdw(12)}^{NL}(w_2-w_1)^3\right)\end{pmatrix}dw_2\,R_2 d\theta dx\end{aligned} \quad (7)$$

$$-\int_0^L\int_0^{2\pi}\int_0^{w_3}\left(\frac{R_2}{R_3}\right)\left(C_{vdw(32)}^{L}(w_3-w_2)+C_{vdw(32)}^{NL}(w_3-w_2)^3\right)dw_3\,R_3 d\theta dx,$$

$$W_{vm}=-\int_0^L\int_0^{2\pi}\int_0^{w_3}\left(K_w w_3-K_p\nabla^2 w_3+C_w\frac{\partial w_3}{\partial t}\right)dw_3 R_3 d\theta dx, \tag{8}$$

$$W_e=\int_0^L\int_0^{2\pi}\int_0^{w_3}\frac{\pi\Upsilon(V_{DC}+V_{AC}\cos(\omega t))^2}{\sqrt{(b_2-w_3)(2R_3+b_3-w_3)}\left[\cosh^{-1}\left(1+\frac{b_3-w_3}{R_3}\right)\right]^2}dw_3\,R_3 d\theta dx, \tag{9}$$

Where all coefficients and phrases of Eqs. (7)- (9) can be seen in reference [11-13]. Also, the external work of the fluid can be written as [24]

$$W_f=\frac{1}{2}\int_0^L\int_0^{2\pi}F_{fluid}\,w\,Rd\theta dx$$

$$=\frac{1}{2}\int_0^L\int_0^{2\pi}\left\{\begin{array}{c}-\rho_f A_f\left(\begin{array}{c}\frac{\partial^2 w}{\partial t^2}+2\left(VCF\times V_{no-slip}\right)\frac{\partial^2 w}{\partial x\partial t}\\+\left(VCF\times V_{no-slip}\right)^2\frac{\partial^2 w}{\partial x^2}\end{array}\right)\\+\mu A_f\left(\begin{array}{c}\frac{\partial^3 w}{\partial x^2\partial t}+\frac{\partial^3 w}{R^2\partial\theta^2\partial t}\\+\left(VCF\times V_{no-slip}\right)\left(\frac{\partial^3 w}{\partial x^3}+\frac{\partial^3 w}{R^2\partial x\partial\theta^2}\right)\end{array}\right)\end{array}\right\}w\,Rd\theta dx \tag{10}$$

By applying of following Hamilton's principle

$$\int_0^t(\delta T_n-\delta\pi_n+\delta w_{vm}+\delta w_{vdw}+\delta w_e)dt=0, \tag{11}$$

and substituting Eqs. (5)- (10) into Eq. (11), the governing equations of motion and boundary conditions for FC-TWPENS respectively are obtained as follows;

$$\delta u_n:\quad\frac{\partial N_{xn}}{\partial x}+\frac{1}{R_n}\frac{\partial N_{x\theta n}}{\partial\theta}=I_n\frac{\partial^2 u_n}{\partial t^2}, \tag{12}$$

$$\delta v_n:\quad\frac{\partial N_{x\theta n}}{\partial x}+\frac{1}{R_n}\frac{\partial N_{\theta n}}{\partial\theta}=I_n\frac{\partial^2 v_n}{\partial t^2}, \tag{13}$$

$$\delta w_n:\quad\frac{\partial^2 M_{xn}}{\partial x^2}+\frac{2}{R_n}\frac{\partial^2 M_{x\theta n}}{\partial x\partial\theta}+\frac{1}{R_n^2}\frac{\partial^2 M_{\theta n}}{\partial\theta^2}-\frac{N_{\theta n}}{R_n}+N_{xn}\frac{\partial^2 w_n}{\partial x^2}+\frac{\partial N_{xn}}{\partial x}\frac{\partial w_n}{\partial x}+\frac{N_{\theta n}}{R_n^2}\frac{\partial^2 w_n}{\partial\theta^2}$$
$$+\frac{1}{R_n^2}\frac{\partial N_{\theta n}}{\partial\theta}\frac{\partial w_n}{\partial\theta}+\frac{2}{R_n}N_{x\theta n}\frac{\partial^2 w_n}{\partial x\partial\theta}+\frac{1}{R_n}\frac{\partial N_{x\theta n}}{\partial x}\frac{\partial w_n}{\partial\theta}+\frac{1}{R_n}\frac{\partial N_{x\theta n}}{\partial\theta}\frac{\partial w_n}{\partial x}=I_n\frac{\partial^2 w_n}{\partial t^2}+S_n \tag{14}$$

$$-\frac{\pi\Upsilon(V_{DC}+V_{AC}\cos(\omega t))^2}{\sqrt{(b_2-w_2)(2R_2+b_2-w_2)}\left[\cosh^{-1}\left(1+\frac{b_2-w_2}{R_2}\right)\right]^2},$$

where $S_n$ for the inner and outer layer, respectively, are:

$$S_1 = -\left(C^{L}_{vdw(12)}(w_2-w_1)+C^{NL}_{vdw(12)}(w_2-w_1)^3\right),) \tag{15a}$$

$$S_2 = \begin{pmatrix} -C^{L}_{vdw(23)}(w_3-w_2)-C^{NL}_{vdw(23)}(w_3-w_2)^3 \\ +\left(\frac{R_1}{R_2}\right)\left(C^{L}_{vdw(12)}(w_2-w_1)+C^{NL}_{vdw(12)}(w_2-w_1)^3\right) \end{pmatrix} \tag{15b}$$

$$S_3 = \begin{pmatrix} \left(\frac{R_2}{R_3}\right)\left(C^{L}_{vdw(32)}(w_3-w_2)+C^{NL}_{vdw(32)}(w_3-w_2)^3\right) \\ +K_w w_3 - K_p\nabla^2 w_3 + C_w\frac{\partial w_3}{\partial t} \end{pmatrix} \tag{15c}$$

and boundary conditions are obtained as follows:

$$\delta u_n = 0 \quad or \quad N_{xn}n_x + \frac{1}{R_n}N_{x\theta n}n_\theta = 0, \tag{16}$$

$$\delta v_n = 0 \quad or \quad N_{x\theta n}n_x + \frac{1}{R_n}N_{\theta n}n_\theta = 0, \tag{17}$$

$$\delta w_n = 0 \quad or \quad \left(\frac{\partial M_{xn}}{\partial x}+\frac{1}{R_n}\frac{\partial M_{x\theta n}}{\partial\theta}+N_{xx}\frac{\partial w_n}{\partial x}+\frac{N_{x\theta}}{R_n}\frac{\partial w_n}{\partial\theta}\right)n_x + \left(\frac{1}{R_n}\frac{\partial M_{x\theta n}}{\partial x}+\frac{1}{R_n^2}\frac{\partial M_{\theta n}}{\partial\theta}+\frac{N_{x\theta n}}{R_n}\frac{\partial w_n}{\partial x}+\frac{N_{\theta n}}{R_n^2}\frac{\partial w_n}{\partial\theta}\right)n_\theta = 0, \tag{18}$$

$$\frac{\partial w_n}{\partial x} = 0 \quad or \quad M_{xn}n_x + \frac{1}{R_n}M_{x\theta n}n_\theta = 0, \tag{19}$$

$$\frac{\partial w_n}{\partial\theta} = 0 \quad or \quad \frac{1}{R_n}M_{x\theta n}n_x + \frac{1}{R_n^2}M_{\theta n}n_\theta = 0, \tag{20}$$

The following dimensional parameters are also used to dimensionless equations of motion and boundary conditions.

$$\bar{u}_n=\frac{u_n}{h_{Nn}},\bar{v}_n=\frac{v_n}{h_{Nn}},\bar{w}_n=\frac{w_n}{h_{Nn}},\xi_n=\frac{x_n}{L},\bar{b}_n=\frac{b_n}{L},\bar{A}_{ijNn}=\frac{A_{ijNn}}{A_{11Nn}},\bar{B}_{ijNn}=\frac{B_{ijNn}}{A_{11Nn}h_{Nn}},$$
$$\bar{D}_{ijNn}=\frac{D_{ijNn}}{A_{11Nn}h_{Nn}^2},\bar{A}_{ijpn}=\frac{A_{ijpn}}{A_{11Nn}},\bar{A}_{ijn}^*=\frac{A_{ijn}^*}{A_{11Nn}},\bar{B}_{ijpn}=\frac{B_{ijpn}}{A_{11Nn}h_{Nn}},\bar{B}_{ijn}^*=\frac{B_{ijn}^*}{A_{11Nn}h_{Nn}},$$
$$\bar{D}_{ijpn}=\frac{D_{ijpn}}{A_{11Nn}h_{Nn}^2},\bar{D}_{ijn}^*=\frac{D_{ijn}^*}{A_{11Nn}h_{Nn}^2},\bar{F}_{11Nn}^*=\frac{F_{11Nn}^*}{A_{11Nn}h_{Nn}},\bar{F}_{11pn}^*=\frac{F_{11pn}^*}{A_{11Nn}h_{Nn}},$$
$$\bar{E}_{11Nn}^*=\frac{E_{11Nn}^*}{A_{11Nn}h_{Nn}^2},\bar{E}_{11pn}^*=\frac{E_{11pn}^*}{A_{11Nn}h_{Nn}^2},\bar{J}_{11Nn}^*=\frac{J_{11Nn}^*}{\rho_{Nn}h_{Nn}^2},J_{11pn}^*=\frac{J_{11pn}^*}{\rho_{Nn}h_{Nn}^2},$$
$$\bar{G}_{11Nn}^*=\frac{G_{11Nn}^*}{\rho_{Nn}h_{Nn}^3},G_{11pn}^*=\frac{G_{11pn}^*}{\rho_{Nn}h_{Nn}^3},\bar{N}_{xpn}^*=\frac{N_{xpn}^*V_0}{A_{11Nn}},\bar{N}_{\theta pn}^*=\frac{N_{\theta pn}^*V_0}{A_{11Nn}},\bar{M}_{xpn}^*$$
$$=\frac{M_{xpn}^*V_0}{A_{11Nn}h_{Nn}},$$
$$\bar{M}_{\theta pn}^*=\frac{M_{\theta pn}^*V_0}{A_{11Nn}h_{Nn}},\bar{\tau}_0^{sn}=\frac{\tau_0^{sn}}{A_{11Nn}},\bar{R}_n=\frac{R_n}{L},m_{0n}=\frac{L}{R_n},m_{1n}=\frac{L}{h_{Nn}},m_{2n}=\frac{h_{Nn}}{R_n}=\bar{h}_{Nn},\quad(21)$$
$$\bar{h}_{pn}=\frac{h_{pn}}{R_n},m_{3n}=\frac{I_n}{2\rho_{Nn}h_{Nn}},m_{4n}=\frac{h_{pn}}{h_{Nn}},\Omega_{\mathrm{n}}=\sqrt{\frac{A_{11Nn}}{2\rho_{Nn}h_{Nn}L^2}},\tau_n=\Omega_{\mathrm{n}}t_n,\bar{\omega}_n=\frac{\omega_n}{\Omega_{\mathrm{n}}},$$
$$\bar{K}_w=\frac{K_wL^2}{m_3A_{11N}},\bar{K}_p=\frac{K_p}{m_3A_{11N}},\bar{C}_{w2}=\frac{C_w\Omega L^2}{m_{3n}A_{11Nn}},\bar{C}_{vdwn}^{L}=\frac{C_{vdwn}^{L}L^2}{m_{3n}A_{11Nn}},$$
$$\bar{C}_{vdwn}^{NL}=\frac{C_{vdwn}^{NL}L^2h_{Nn}^2}{m_{3n}A_{11Nn}},\bar{\rho}_f=\frac{\rho_f}{m_3\rho_N},\bar{u}_f=\left(VCF\times V_{no-slip}\right)\sqrt{\frac{2\rho_Nh_N}{A_{11N}}},$$
$$\bar{\mu}_f=\frac{\mu_f}{m_3}\sqrt{\frac{2h_N}{\rho_NA_{11N}L^2}},\bar{V}_{DC}=\frac{V_{DC}}{V_0},\bar{V}_{p2}=\frac{V_{p2}}{V_0},\bar{F}_e=\frac{\pi m_1^2V_0^2\Upsilon}{m_3A_{11N}},$$

In current study, the electrostatic force Eq. (9) can be expressed as a polynomial form that is solved by nonlinear curve-fitting problem of lsqcurvefit function in Matlab Toolbox using least-squares. Therefore, the dimensionless electrostatic work can be written as follows [13]:

$$W_e=\int_0^L\int_0^{2\pi}\int_0^{\bar{w}_3}\bar{F}_e(\bar{V}_{DC}+\bar{V}_{AC}\cos(\bar{\omega}\tau))^2\begin{pmatrix}\bar{C}_1+\bar{C}_2\bar{w}_3+\bar{C}_3\bar{w}_3^2\\+\cdots+\bar{C}_n\bar{w}_3^{n-1}\end{pmatrix}d\bar{w}_3\,\bar{R}_3d\theta d\xi \quad (22)$$

**2-3: Solution procedure**

By using the following shear deformation and displacement in the assumed mode method [11-13]

$$\begin{bmatrix}u_n(x,\theta,t)\\v_n(x,\theta,t)\\w_n(x,\theta,t)\end{bmatrix}=\sum_{m=1}^{M_1}\sum_{j=1}^{N}\begin{bmatrix}\left[u_{m,j,c}(\tau)\cos(j\theta)+u_{m,j,s}(\tau)\sin(j\theta)\right]\chi_{mj}(\xi)\\\left[v_{m,j,c}(\tau)\sin(j\theta)+v_{m,j,s}(\tau)\cos(j\theta)\right]\phi_{mj}(\xi)\\\left[w_{m,j,c}(\tau)\cos(j\theta)+w_{m,j,s}(\tau)\sin(j\theta)\right]\beta_{mj}(\xi)\end{bmatrix} \quad (23)$$

$$+\sum_{m=1}^{M_2}\begin{bmatrix}u_{m,0}(\tau)\chi_{m0}(\xi)\\ v_{m,0}(\tau)\phi_{m0}(\xi)\\ w_{m,0}(\tau)\beta_{m0}(\xi)\end{bmatrix}=\sum_{(i,r,s)=1}^{M_2+M_1\times N}\begin{bmatrix}u_{ni}(\tau)\chi_{ni}(\xi)\vartheta_{ni}(\theta)\\ v_{nr}(\tau)\phi_{nr}(\xi)\alpha_{nr}(\theta)\\ w_{ns}(\tau)\beta_{ns}(\xi)\psi_{ns}(\theta)\end{bmatrix},$$

And using dimensionless strain and kinetic energies Eqs. (5) and (6) and dimensionless applied works Eqs. (7)- (9) and substituting of the Lagrange-Euler equations, the following reduced-order model of the nonlinear equations of motion are obtained:

$$[(M)_u^u]_n\{\ddot{\bar{u}}_n\}+[(M)_u^w]_n\{\ddot{\bar{w}}_n\}+[(K)_u^u]_n\{\bar{u}_n\}+[(K)_u^v]_n\{\bar{v}_n\}+[(K)_u^w]_n\{\bar{w}_n\}+[(NL)_u^w]_n\{\bar{w}_n^2\}=\bar{F}_{un}, \tag{24}$$

$$[(M)_v^v]_n\{\ddot{\bar{v}}_n\}+[(M)_v^w]_n\{\ddot{\bar{w}}_n\}+[(K)_v^v]_n\{\bar{v}_n\}+[(K)_v^u]_n\{\bar{u}_n\}+[(K)_v^w]_n\{\bar{w}_n\}+[(NL)_v^w]_n\{\bar{w}_n^2\}=\bar{F}_{vn}, \tag{25}$$

$$\left[[(M)_w^w]_n+\left[(K)_{w2}^{\ddot{w}}\right]_n\{\bar{w}_n\}\right]\{\ddot{\bar{w}}_n\}+[(c)_w^w]\{\dot{\bar{w}}_n\}+[(K)_w^u]_n\{\bar{u}_n\}+[(K)_w^v]_n\{\bar{v}_n\} \tag{26}$$

$$+[[(K)_w^w]_n-\bar{F}_{e2}(K_e)_w^w]\{\bar{w}_n\}$$

$$+(-1)^n q_1\left(\frac{\bar{R}_{n-1}}{\bar{R}_n}\right)^{m_1}\bar{C}^{\,L}_{vdw((n-1)n)}\left([(K)_{w1n}^{vdw}]\{\bar{w}_n\}-[(K)_{w2n}^{vdw}]\{\bar{w}_{n-1}\}\right)$$

$$+(-1)^n q_2\left(\frac{\bar{R}_n}{\bar{R}_{n+1}}\right)^{m_2}\bar{C}^{\,L}_{vdw(n(n+1))}\left([(K)_{w3n}^{vdw}]\{\bar{w}_{n+1}\}-[(K)_{w4n}^{vdw}]\{\bar{w}_n\}\right)$$

$$+(-1)^n q_1\left(\frac{\bar{R}_{n-1}}{\bar{R}_n}\right)^{m_1}\left(\bar{C}^{\,NL}_{vdw((n-1)n)}\right)\begin{pmatrix}[(NL)_{w1n}^{vdw}]\bar{w}_n^3-3[(NL)_{w2n}^{vdw}]\bar{w}_n^2\bar{w}_{n-1}\\ +3[(NL)_{w3n}^{vdw}]\bar{w}_n\bar{w}_{n-1}^2-[(NL)_{w4n}^{vdw}]\bar{w}_{n-1}^3\end{pmatrix}$$

$$+(-1)^n q_2\left(\frac{\bar{R}_n}{\bar{R}_{n+1}}\right)^{m_2}\left(\bar{C}^{\,NL}_{vdw(n(n+1))}\right)\begin{pmatrix}\left[(NL)_{w5n}^{vdw}\right]\bar{w}_{n+1}^3-3[(NL)_{w6n}^{vdw}]\bar{w}_{n+1}^2\bar{w}_n\\ +3[(NL)_{w7n}^{vdw}]\bar{w}_{n+1}\bar{w}_n^2-[(NL)_{w8n}^{vdw}]\bar{w}_n^3\end{pmatrix}$$

$$+[(NL)_w^u]\{\bar{w}_n\bar{u}_n\}+[(NL)_w^v]\{\bar{w}_n\bar{v}_n\}+[(NL)_{w2}^w-\bar{F}_{e3}(NL_{2e})_w^w]\{\bar{w}_n^2\}$$

$$+[(NL)_{w3}^w-\bar{F}_{e4}(NL_{3e})_w^w]\{\bar{w}_n^3\}=\bar{F}_{we}+\bar{F}_{wn}$$

$$+\bar{F}_e\{((\bar{V}_{AC}cos\bar{\omega}\tau)^2+2\bar{V}_{AC}\bar{V}_{DC}cos\bar{\omega}\tau)(\bar{C}_4(NL_{3e})_w^w+\bar{C}_3(NL_{2e})_w^w+\bar{C}_2(K_e)_w^w+\bar{C}_1\bar{F}_1)\}$$

In Eq. (26), for $n=1$: $m_2=q_1=0$ ; $q_2=1$; for $n=2$: $m_2=0$; $m_1=q_1=1$; $q_2=-1$;and for $n=3$: $q_2=0; m_1=1$; $q_1=-1$. Also, $[(K)_w^{vdw}]_n$ is stiffness matrix for van der Walls effect. All coefficients of Eqs. (24) - (26) are presented in Appendix 1 and 2.

**3: Results and Discussions**

Verification study is investigated in reference Hashemi Kachapi et al. [11-13] with full details for SW and DW piezoelectric nanostructures. In this section, the effects of surface/interface parameters of FC-MWPENS such as Lame's constants ($\lambda^{I,S},\mu^{I,S}$), residual stress ($\tau_0^{I,S}$), piezoelectric constants

($e_{31p}^{s_k}, e_{32p}^{s_k}$) and mass density ($\rho^{I,S}$) is investigated for analysis of dimensionless natural frequency respect to viscous fluid velocity $\bar{u}_f$ and pull-in voltage $\bar{V}_{DC}$. In order to simplify the presentation, CC, SS and CS represent clamped edge, simply supported edge and clamped-simply supported edge, respectively. The material properties for the different layers of Aluminum nanoshell (Al) and piezoelectric layer (PZT-4) are shown in Tables 1 and 2, respectively [11, 13].

**Table 1.** Surface and bulk properties of Al

| $E_N(GPa)$ | $\upsilon_N$ | $\rho_N(kg/m^3)$ | $\lambda^I(N/m)$ | $\mu^I(N/m)$ | $\tau_0^I(N/m)$ | $\rho^I(kg/m^2)$ |
|---|---|---|---|---|---|---|
| 70 | 0.33 | 2700 | 3.786 | 1.95 | 0.9108 | $5.46\times10^{-7}$ |

**Table 2.** Surface and bulk properties of PZT-4

| $C_{11p}(GPa)$ | $C_{22p}(GPa)$ | $C_{12p}(GPa)$ | $C_{21p}(GPa)$ | $C_{66p}(GPa)$ | $E_p(GPa)$ |
|---|---|---|---|---|---|
| 139 | 139 | 77.8 | 77.8 | 30.5 | 95 |
| $\upsilon_p$ | $\rho_p(kg\ m^{-3})$ | $\eta_{33p}(10^{-8}\ F/m)$ | $\lambda^S(N/m)$ | $\mu^S(N/m)$ | $\tau_0^S(N/m)$ |
| 0.3 | 7500 | 8.91 | 4.488 | 2.774 | 0.6048 |
| $e_{31p}(C/m^2)$ | $e_{32p}(C/m^2)$ | $e_{31p}^S(C/m)$ | $e_{32p}^S(C/m)$ | $\rho^S(kg/m^2)$ | |
| $-5.2$ | $-5.2$ | $-3\times10^{-8}$ | $-3\times10^{-8}$ | $5.61\times10^{-6}$ | |

The others geometrical parameters for bulk and surface of FC-MWPENS in all following results are shown in Table 3 [11, 13].

**Table 3.** The material and geometrical parameters

| $R_1(m)$ | $R_2(m)$ | $R_2(m)$ | $L/R_1$ | $h_{N_{(1,2,3)}}/R_1$ |
|---|---|---|---|---|
| $1\times10^{-9}$ | $1.5\times10^{-9}$ | $2\times10^{-9}$ | 10 | 0.01 |
| $h_{p_3}/R_1$ | $b_3/R_3$ | $K_{w_3}(N/m^3)$ | $K_{p_3}(N/m)$ | $V_{p_3}(V)$ |
| 0.005 | 0.1 | $8.9995035\times10^{17}$ | 2.071273 | $1\times10^{-3}$ |
| $C_{w_3}(N.S/m)$ | $C_{vdw_3}^L(N/m^3)$ | $C_{vdw_3}^{NL}(N/m^3)$ | $V_{03}$ | $V_{DC_3}(V)$ |
| $1\times10^{-3}$ | $9.91866693\times10^{19}$ | $2.201667\times10^{31}$ | 1 | 5 |
| $\mu_f(pa.s)$ | $\rho_f(kg/m^3)$ | $u_f(m/s)$ | | |
| $3\times10^{-3}$ | 1060 | 50 | | |

Where the value of the mid-surface radius for different PENS are presented as following:

for SWPENS: $R = R_{out}$; for DWPENS: $R_1 = R_{in}, R_2 = R_{out}$;

and for TWPENS: $R_1 = R_{in}, R_2 = R_{mid}, R_3 = R_{out}$.

### 3-1: Surface/interface effects on DNF respect to viscous fluid velocity and pull-in voltage

In this section, the effect of surface/interface parameters of fluid-conveying multi walled piezoelectric nano-sensor such as Lame's constants ($\lambda^{I,S}, \mu^{I,S}$), residual stress ($\tau_0^{I,S}$), piezoelectric constants ($e_{31p}^{s_k}, e_{32p}^{s_k}$) and mass density ($\rho^{I,S}$) are studied for analysis of dimensionless natural frequency respect to viscous fluid velocity $\bar{u}_f$ and pull-in voltage $\bar{V}_{DC}$. For this work, the material and geometrical parameters in Tables 1-3 are used. In all following results, in analysis of DNF on viscous fluid velocity $\bar{u}_f$ and pull-in voltage $\bar{V}_{DC}$, respectively are used values of $\bar{V}_{DC} = 5$ and $\bar{u}_f = 0.1$.

First, the relationship between the DNF and the different MWPENR length to radius ratio $L/R_1$ is shown in Figure 2 for three vibrational modes. This results show for two case of surface density corresponding to Table 4 (due to the surface/interface densities play an important role in analysis of natural frequency and nonlinear frequency response).

**Table 4.** Two case of surface density.

| Case 1 | | Case 2 | |
|---|---|---|---|
| $\rho^I(kg/m^2)$ | $\rho^S(kg/m^2)$ | $\rho^I(kg/m^2)$ | $\rho^S(kg/m^2)$ |
| $5.46 \times 10^{-7}$ | $5.61 \times 10^{-6}$ | $5.46 \times 10^{-8}$ | $5.61 \times 10^{-7}$ |

It is observed that for all modes, the DNF decreases when the $L/R_1$ ratio increases. Also, the DNF for mode 3 is higher than that for modes 1 and 2. It is clear from this Figure that in the case of higher surface/interface densities (case 1), the inertia of the shell is increased and its stiffness is reduced that leads to decreasing of the DNF compared to case of without S/I effects. Also, with decreasing of surface/interface densities (case 2), the inertia of the system is increased and with increase of stiffness, DNF increases compared to case of without S/I effects.

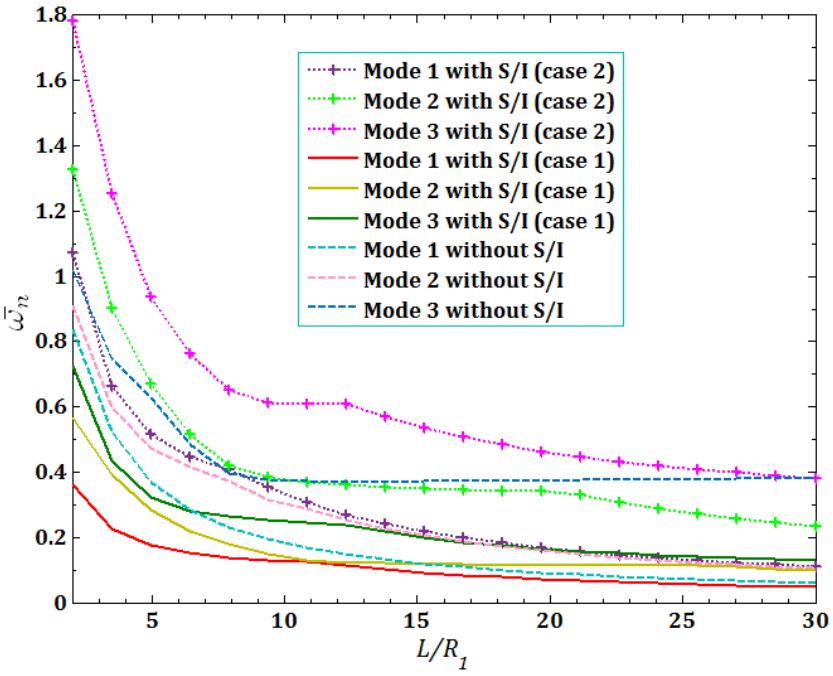


**Fig.2.** The surface/ interface effects on DNF versus $L/R_1$ ratio for three vibrational modes

In all following results, lower surface/interface densities case 2 is used in analysis of DNF on viscous fluid velocity $\bar{u}_f$ and pull-in voltage $\bar{V}_{DC}$.

The effects of viscous fluid velocity $\bar{u}_f$ and direct pull in voltage DC as pull-in instability analysis on the DNF $(\bar{\omega}_n)$ of FC-MWPENS are presented in Figures 3 and 4 and for different boundary conditions. It can be seen that in all boundary conditions, natural frequencies decrease with increasing of fluid velocity and voltage DC. Also, due to the system softening in SS boundary condition with and without S/I and low natural frequency in this case, FC-MWPENS is at a higher critical fluid velocity and lower pull in voltage than other boundary conditions. After SS boundary condition, respectively, CS and CC boundary conditions reach the zero due to being softer. For zero natural frequency, FC-MWPENS becomes unstable and this physically implies that the FC-MWPENS losses its stability due to the divergence via a pitchfork bifurcation.

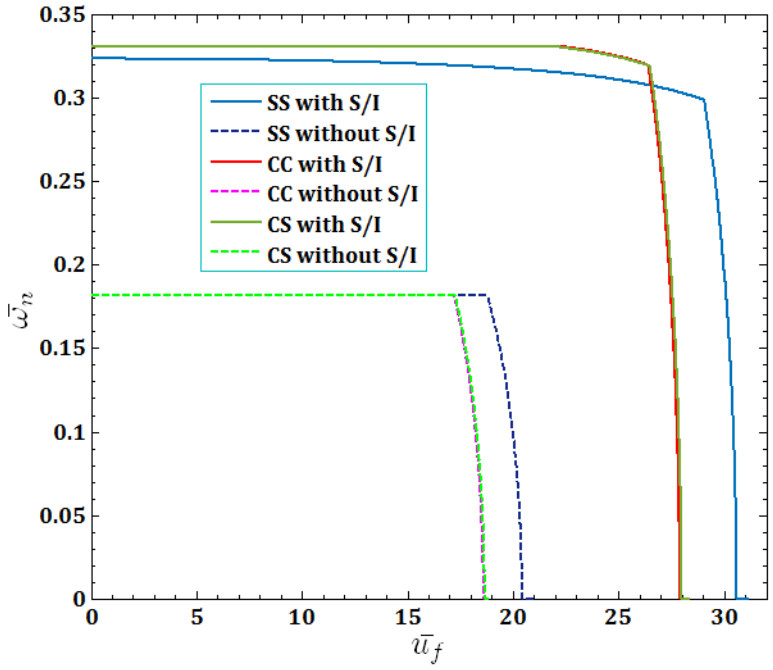


**Fig. 3.** The effects of different boundary conditions for fluid velocity $\bar{u}_f$ on DNF of FC-MWPENS

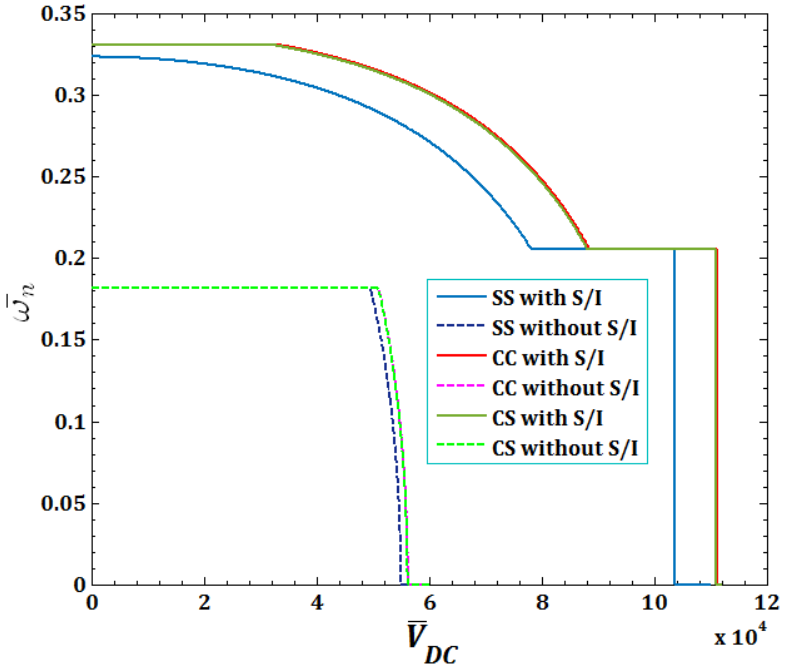


**Fig. 4**. The effects of different boundary conditions for pull in voltage on DNF of FC-MWPENS

Figures 5 and 6 illustrate the effects of different surface and interface Lame's constants $\lambda^{S_k}$ and $\lambda^{I_k}$, for viscous fluid velocity $\bar{u}_f$ and pull-in instability analysis on DNF of FC-MWPENS. It is clear that increasing both surface/interface Lame's constants $\lambda^{I,S}$, due to increasing of FC-MWPENS stiffness, DNF and critical fluid velocity increase and pull in voltage in $\lambda^{I,S} = 0$ and $\lambda^{I,S} = -2$ has maximum and minimum value.

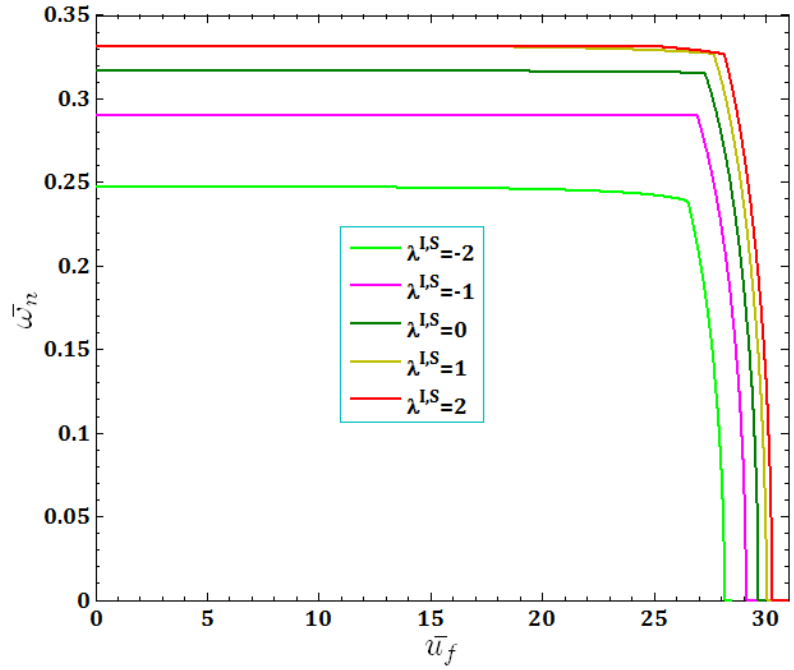


**Fig. 5.** The effects of surface/interface Lame's constants $\lambda^{I,S}$ for fluid velocity $\bar{u}_f$ on DNF of SS FC-MWPENS

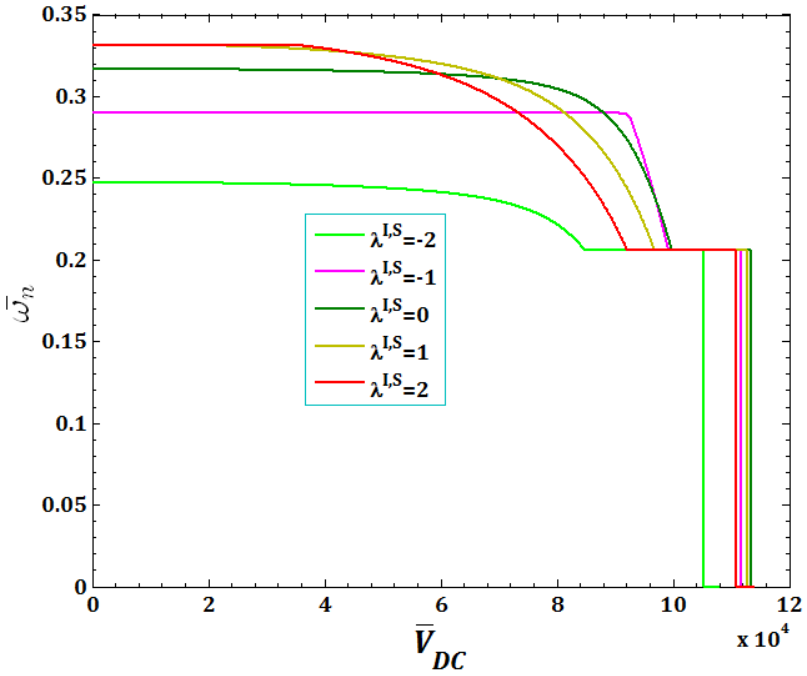


**Fig. 6.** The effects of surface/interface Lame's constants $\lambda^{I,S}$ for pull in voltage on DNF of SS FC-MWPENS

The effects of different surface and interface Lame's constants $\mu^{S_k}$, and $\mu^{I_k}$, for viscous fluid velocity $\bar{u}_f$ and pull-in instability analysis on DNF of FC-MWPENS are presented in Figures 7 and 8. Similar to $\lambda^{I,S}$, it is clear that increasing both surface/interface Lame's constants $\mu^{I,S}$, due to increasing of FC-MWPENS stiffness, DNF and also critical fluid velocity and pull-in voltage increase.

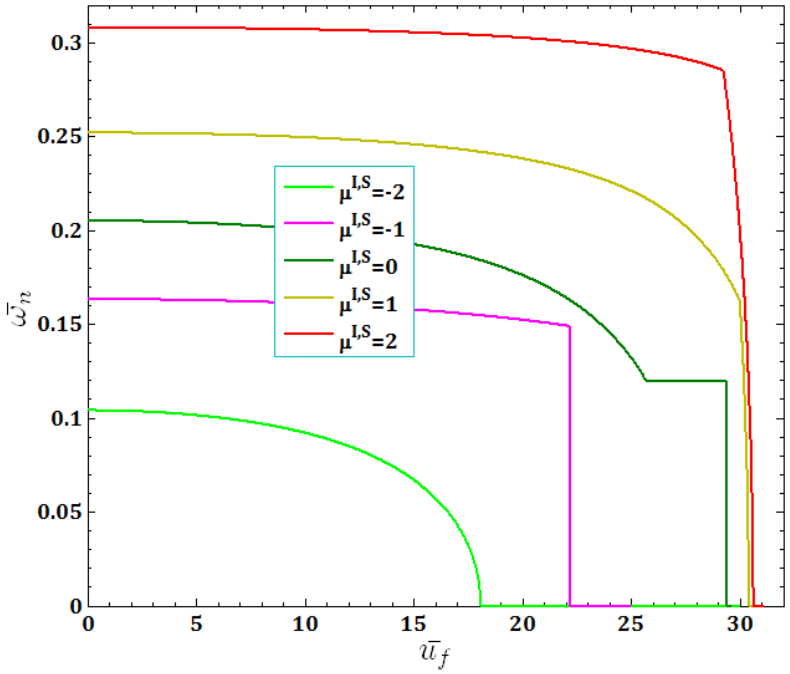


**Fig. 7.** The effects of surface/interface Lame's constants $\mu^{I,S}$ for fluid velocity $\bar{u}_f$ on DNF of SS FC-MWPENS

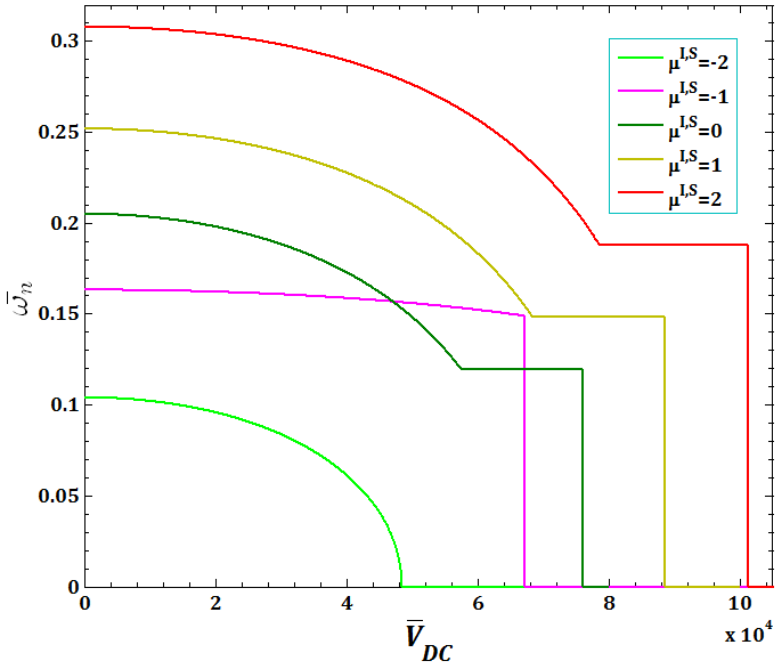


**Fig. 8.** The effects of surface/interface Lame's constants $\mu^{I,S}$ for pull in voltage on DNF of SS FC-MWPENS

Figures 9 and 10 show the effects of surface and interface residual stress $\tau_0^{S_k}$ and $\tau_0^{I_k}$, for viscous fluid velocity $\bar{u}_f$ and pull-in instability analysis on DNF of FC-MWPENS. As can be show in both analysis of DNF and NDR, increasing both surface/interface residual stress $\tau_0^{I,S}$ lead to increasing of FC-MWPENS stiffness and as a result, DNF and pull-in voltage decrease and critical fluid velocity increase.

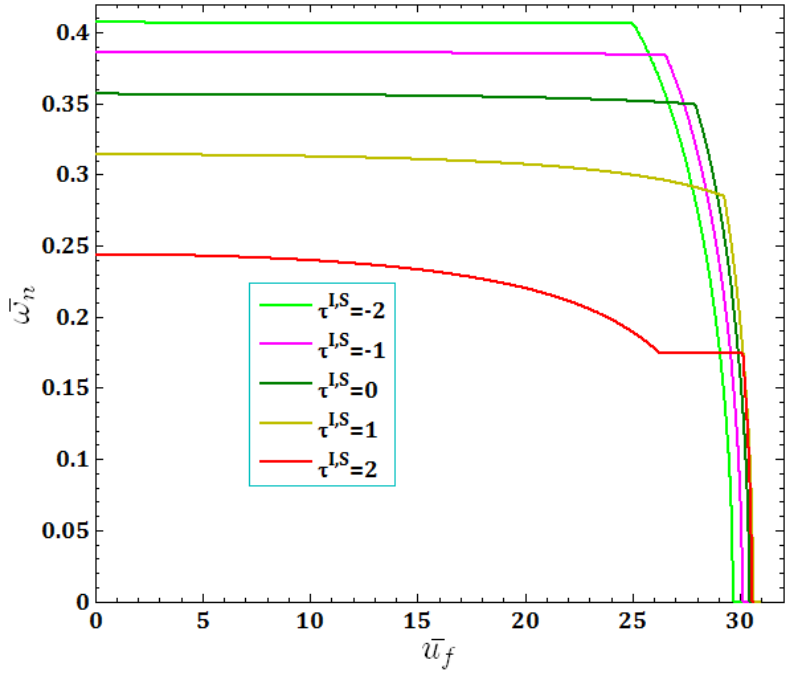


**Fig. 9.** The effects of surface/interface residual stress $\tau_0^{I,S}$ for fluid velocity $\bar{u}_f$ on DNF of SS FC-MWPENS

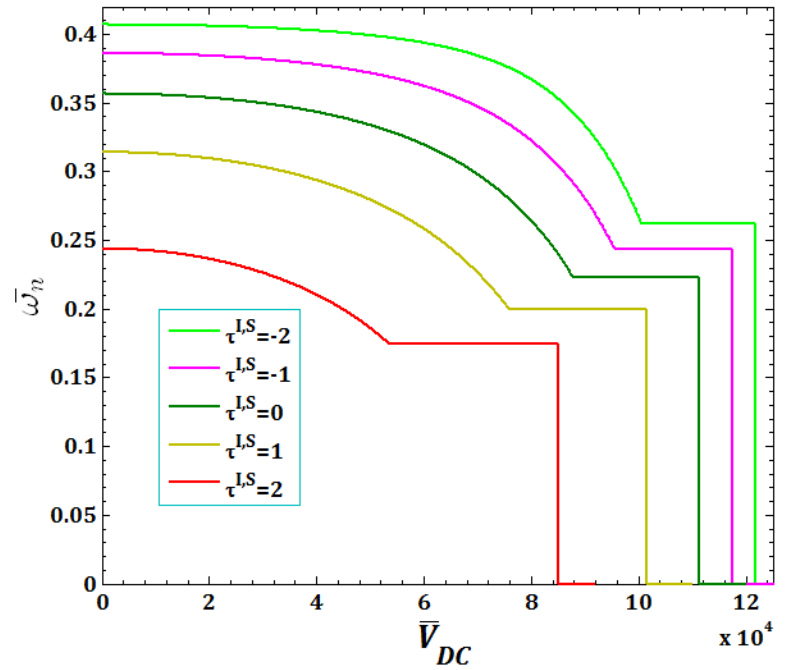


**Fig. 10.** The effects of surface/interface residual stress $\tau_0^{I,S}$ for pull in voltage on DNF of SS FC-MWPENS

The effect of surface piezoelectricity constants $e_{31p}^{s_k}$ and $e_{32p}^{s_k}$ for viscous fluid velocity $\bar{u}_f$ and pull-in instability analysis on DNF of FC-MWPENS is presented in Figures 11 and 12. It is observed that increasing of negative surface piezoelectricity constants $e_{31p}^{s_k}$ and $e_{32p}^{s_k}$ leads to increasing of the FC-MWPENS stiffness and as a result, DNF, critical fluid velocity and pull-in voltage increase.

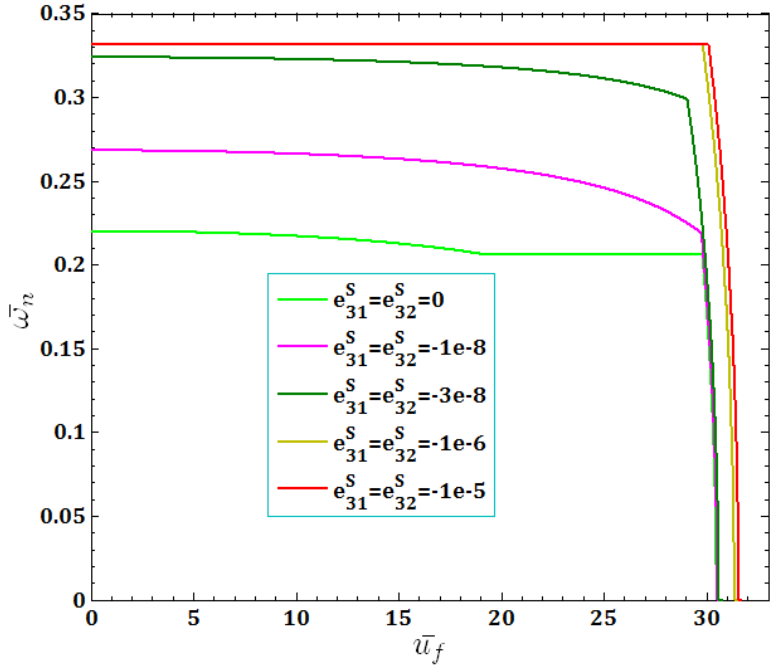


**Fig. 11.** The effects of surface piezoelectricity constants $e_{31p}^{S_k}, e_{32p}^{S_k}$ for fluid velocity $\bar{u}_f$ on DNF of SS FC-MWPENS

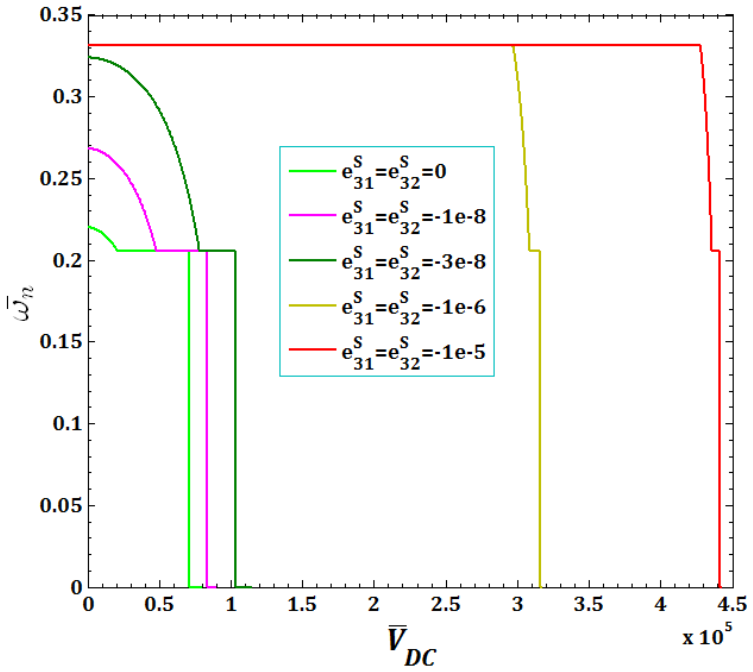


**Fig. 12.** The effects of surface piezoelectricity constants $e_{31p}^{S_k}, e_{32p}^{S_k}$ for pull in voltage on DNF of SS FC-MWPENS

Figures 13 and 14 illustrate the effects of surface and interface mass density $\rho^{S_k}$ and $\rho^{I_k}$, for viscous fluid velocity $\bar{u}_f$ and pull-in instability analysis on DNF of FC-MWPENS. As it can be seen that with increasing surface/interface mass density $\rho^{I,S}$, due to decreasing of the FC-MWPENS stiffness, DNF significantly decrease and also critical fluid velocity and pull-in voltage slightly decrease.

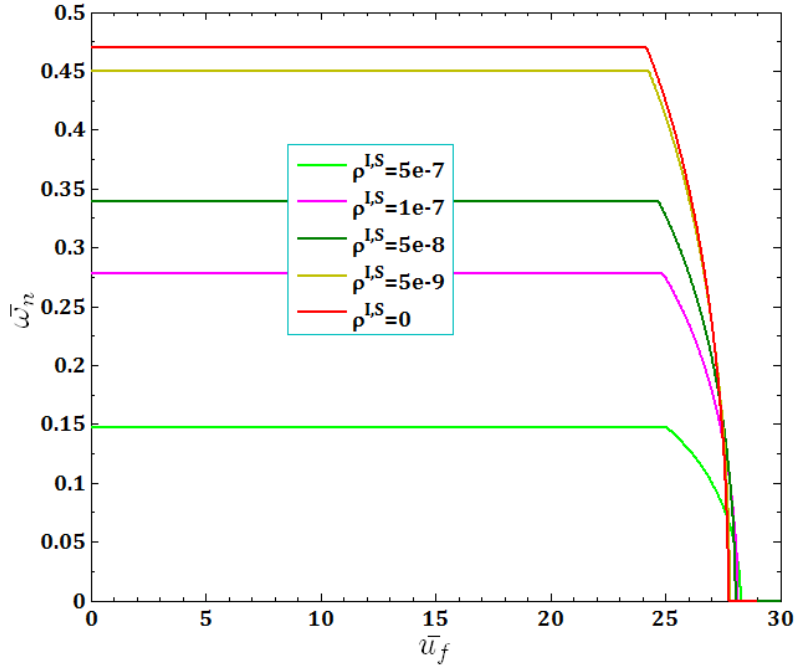


**Fig. 13.** The effect of surface $\rho^S$ and Interface $\rho^I$ mass density for fluid velocity $\bar{u}_f$ on DNF of SS FC-MWPENS

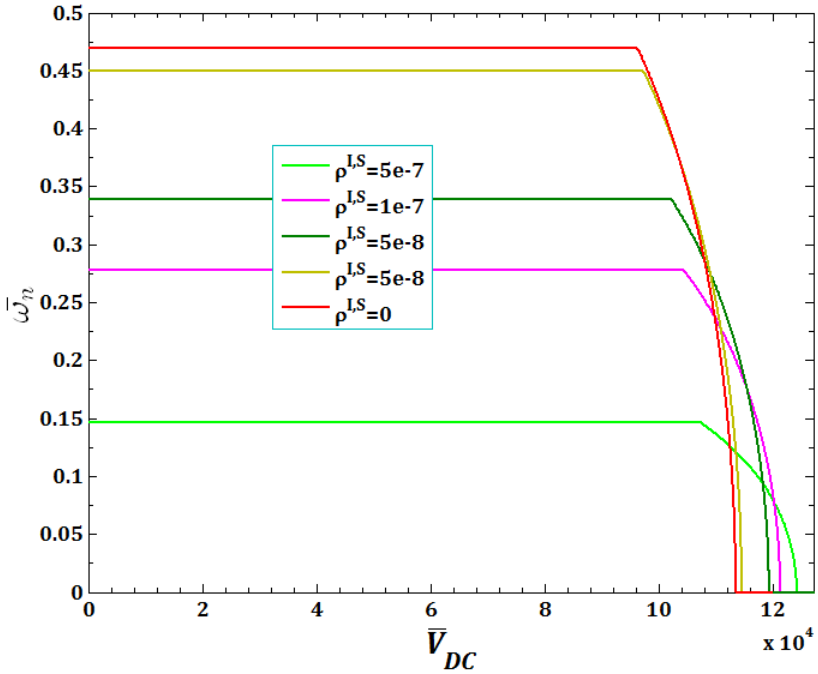


**Fig. 14.** The effect of surface $\rho^S$ and Interface $\rho^I$ mass density for pull in voltage on DNF of SS FC-MWPENS

In Figure 15 and 16 the effects of all surface and interface parameters for viscous fluid velocity $\bar{u}_f$ and pull-in instability analysis on DNF of SS FC-MWPENS are presented It can be seen that with ignoring the surface/interface density $\rho^{I,S}$, the inertia of the system will greatly decrease and due to increasing of FC-MWPENS stiffness, the system will have a maximum DNF compared to other cases. Also when the surface/interface effects are not taken into account, due to decreasing of nanoshell stiffness, it has a lower DNF than the case of with all S/I effects. In cases of without all S/I effects,

the critical fluid velocity and also pull in voltage, sooner than the rest parameters are reached to be zero and in cases of without surface/interface density $\rho^{I,S}$ and with all S/I effects respectively, pull in voltage and critical fluid velocity later than the rest parameters are reached to be zero and system losses its stability due to the divergence via a pitchfork bifurcation.

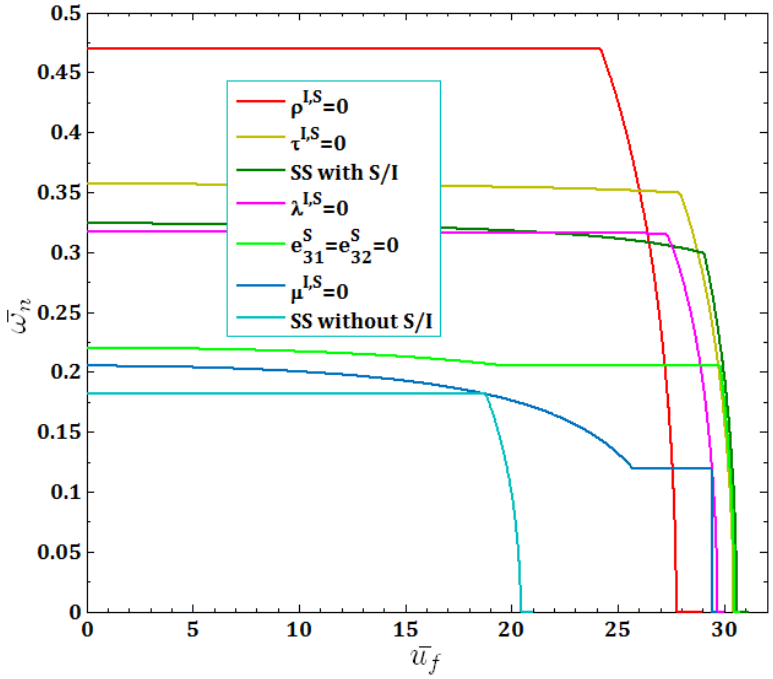


**Fig. 15.** The effects of surface and interface parameters for fluid velocity $\bar{u}_f$ on DNF of SS FC-MWPENS

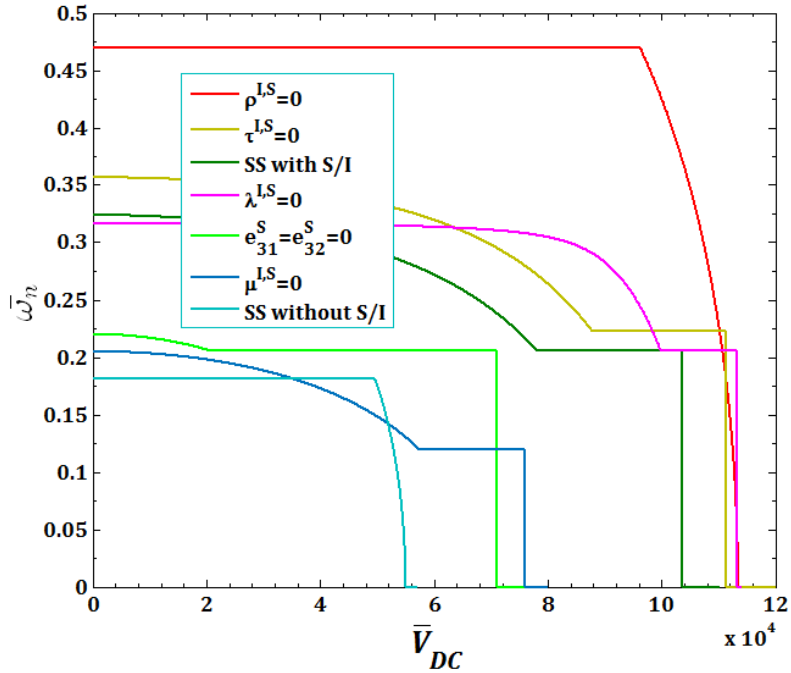


**Fig. 16.** The effects of surface and interface parameters for pull in voltage on DNF of SS FC-MWPENS

## 4. Conclusion

In current study, the effect of surface/interface parameters of fluid-conveying multi walled piezoelectric nano-sensor such as Lame's constants ($\lambda^{I,S}, \mu^{I,S}$), residual stress ($\tau_0^{I,S}$), piezoelectric constants ($e_{31p}^{s_k}, e_{32p}^{s_k}$) and mass density ($\rho^{I,S}$) are studied for analysis of dimensionless natural frequency respect to viscous fluid velocity $\bar{u}_f$ and pull-in voltage $\bar{V}_{DC}$. The piezoelectric nano-sensor is simultaneously subjected to direct electrostatic voltage DC with nonlinear excitation, nonlinear van der Waals force and viscoelastic foundation. For this purpose, Hamilton's principles, the assumed mode method combined with Lagrange–Euler's are used. The validation of the mention system is achieved with excellent agreements by comparisons with numerical results. Some conclusions are obtained from this study:

- in the case of higher (lower) surface/interface densities, the inertia of the shell is increased (decreased) and its stiffness is reduced (increase) that leads to decreasing (increasing) of the natural frequency compared to case of without S/I effects.
- for all modes, the DNF decreases when the $L/R_1$ ratio increases. Also, the DNF for mode 3 is higher than that for modes 1 and 2.
- in all boundary conditions, natural frequencies decrease with increasing of fluid velocity and voltage DC. Also, due to the system softening in SS boundary condition and low natural frequency in this case, FC-MWPENS is a higher critical fluid velocity and lower pull in voltage than other boundary conditions.
- increasing both surface/interface Lame's constants $\lambda^{I,S}$, due to increasing of FC-MWPENS stiffness, DNF and critical fluid velocity increase and pull in voltage in $\lambda^{I,S} = 0$ and $\lambda^{I,S} = -2$ has maximum and minimum value.
- increasing both surface/interface Lame's constants $\mu^{I,S}$, due to increasing of FC-MWPENS stiffness, DNF and also critical fluid velocity and pull-in voltage increase.
- in both analysis of DNF and NDR, increasing both surface/interface residual stress $\tau_0^{I,S}$ lead to increasing of FC-MWPENS stiffness and as a result, DNF and pull-in voltage decrease and critical fluid velocity increase.
- increasing of negative surface piezoelectricity constants $e_{31p}^{s_k}$ and $e_{32p}^{s_k}$ leads to increasing of the FC-MWPENS stiffness and as a result, DNF, critical fluid velocity and pull-in voltage increase.
- increasing surface/interface mass density $\rho^{I,S}$, due to decreasing of the FC-MWPENS stiffness, DNF significantly decrease and also critical fluid velocity and pull-in voltage slightly decrease.
- with ignoring the surface/interface density $\rho^{I,S}$, the system will have a maximum DNF compared to other cases.
- when the surface/interface effects are not taken into account, it has a lower DNF than the case of with all S/I effects.
- In cases of without all S/I effects, the critical fluid velocity and also pull in voltage, sooner than the rest parameters are reached to be zero and in cases of without surface/interface density $\rho^{I,S}$ and with all S/I effects respectively, pull in voltage and critical fluid velocity later than the rest parameters are reached to be zero.

**Conflict of interest**

The authors report no conflict of interest.

**Funding Acknowledgement**
'This research received no specific grant from any funding agency in the public, commercial, or not-for-profit sectors'.

**Appendix 1**

$$(M)^{u}_{un} = \iint \left(\chi_e \chi_i \vartheta_f \vartheta_j\right) d\xi \, d\theta \,, \qquad (K)^{u}_{un} = \iint \left(\alpha_{1n} \chi'_{\mathrm{e}} \chi'_{\mathrm{i}} \vartheta_f \vartheta_j + \alpha_{2n} \chi_e \chi_i \vartheta'_f \vartheta'_j\right) d\xi \, d\theta,$$

$$(K)^{v}_{un} = \frac{1}{2} \iint \left(\alpha_{3n} \chi'_{\mathrm{e}} \phi_k \vartheta_f \alpha'_l + \alpha_{4n} \chi_e \phi'_k \vartheta'_f \alpha_l\right) d\xi \, d\theta \,, \qquad (K)^{w}_{un} = \frac{1}{2} \iint \left(\alpha_{5n} \chi'_{\mathrm{e}} \beta_o \vartheta_f \psi_l\right) d\xi \, d\theta,$$

$$(NL)^{w}_{un} = \frac{1}{2} \iint \left(\alpha_{6n} \chi'_{\mathrm{e}} \beta'_0 \beta'_t \vartheta_f \psi_p \psi_v + \alpha_{7n} \chi'_{\mathrm{e}} \beta_o \beta_t \vartheta_f \psi'_p \psi'_v + \alpha_{8n} \chi_e \beta'_0 \beta_t \vartheta'_f \psi_p \psi'_v\right) d\xi \, d\theta,$$

$$\bar{F}_{upn} = \frac{1}{2} \iint \left(\alpha_{26n} \chi'_{\mathrm{e}} \vartheta_i\right) d\xi \, d\theta, \qquad (M)^{v}_{vn} = \iint \left(\phi_q \phi_k a_f a_l\right) d\xi \, d\theta$$

$$(K)^{u}_{vn} = \frac{1}{2} \iint \left(\alpha_{3n} \phi_q \chi'_{\mathrm{i}} \alpha'_f \vartheta_l + \alpha_{4n} \phi'_q \chi_i \alpha_f \vartheta'_l\right) d\xi \, d\theta,$$

$$(K)^{v}_{vn} = \iint \left(\alpha_{9n} \phi_q \phi_k \alpha'_f \alpha'_l + \alpha_{13n} \phi'_q \phi'_k \alpha_f \alpha_l\right) d\xi \, d\theta,$$

$$(K)^{w}_{vn} = \frac{1}{2} \iint \left(\alpha_{12n} \phi_q \beta_o \alpha'_f \psi_l\right) d\xi \, d\theta,$$

$$(NL)^{w}_{vn} = \frac{1}{2} \iint \left(\alpha_{10n} \phi_q \beta_o \beta_t \alpha'_g \psi'_p \psi'_v + \alpha_{11n} \phi_q \beta'_0 \beta'_t \alpha'_g \psi_p \psi_v + \alpha_{14n} \phi'_q \beta'_0 \beta_t \alpha_g \psi_p \psi'_v\right) d\xi \, d\theta,$$

$$\bar{F}_{vpn} = \frac{1}{2} \iint \left(\alpha_{27n} \phi_q \alpha'_f\right) d\xi \, d\theta,$$

$$(M)^{w}_{wn} = \frac{1}{2} \iint \left(2\beta_r \beta_o \psi_s \psi_p + \alpha_{32n} \beta''_r \beta_o \psi_s \psi_p + \alpha_{33n} \beta_r \beta_o \psi''_s \psi_p + \bar{\rho}_{1n} \beta_r \beta_o \psi_s \psi_p\right) d\xi \, d\theta,$$

$$(C)^{w}_{wn} = \frac{1}{2} \iint \left(\bar{C}_{wn} \beta_r \beta_o \psi_s \psi_p + \bar{\rho}_{2n} \beta_r \beta'_o \psi_s \psi_p - \bar{\mu}_{1n} \beta_r \beta''_o \psi_s \psi_p - \bar{\mu}_{2n} \beta_r \beta_o \psi_s \psi''_p\right) d\xi \, d\theta,$$

$$(K)^{u}_{wn} = \frac{1}{2} \iint \left(\alpha_{5n} \beta_r \chi'_{\mathrm{i}} \psi_s \vartheta_j\right) d\xi \, d\theta,$$

$$(K)^{v}_{wn} = \frac{1}{2} \iint \left(\alpha_{12n} \beta_r \phi_k \psi_s \alpha'_l\right) d\xi \, d\theta,$$

$$(K)^{w}_{wn} = \frac{1}{2} \iint \begin{pmatrix} 2\alpha_{15n} \beta_r \beta_o \psi_s \psi_p + 2\alpha_{21n} \beta''_r \beta''_0 \psi_s \psi_p + 2\alpha_{22n} \beta_o \beta_r \psi''_s \psi''_p \\ +2\alpha_{23n} \beta'_r \beta'_o \psi'_s \psi'_p + \alpha_{24n} \beta_r \beta''_o \psi''_s \psi_p + \alpha_{24n} \beta''_r \beta_o \psi_s \psi''_p \\ +2\alpha_{28n} \beta'_r \beta'_o \psi_s \psi_p + \bar{k}_w \beta_r \beta_o \psi_s \psi_p - \bar{k}_p \beta_r \beta''_0 \psi_s \psi_p \\ -\bar{k}_p m_0^2 \beta_r \beta_o \psi_s \psi''_p - \bar{F}_{e2} (K_e)^{w}_{w} \\ +\bar{\rho}_{3n} \beta_r \beta''_0 \psi_s \psi_p - \bar{\mu}_{3n} \beta_r \beta'''_0 \psi_s \psi_p - \bar{\mu}_{4n} \beta_r \beta'_0 \psi_s \psi''_p \end{pmatrix} d\xi \, d\theta,$$

$$(K_e)^{w}_{wn} = \beta_r \beta_o \psi_s \psi_p,$$

$$(K)^{vdw}_{win} = \frac{1}{2} \iint \left(\beta_r \beta_o \psi_s \psi_p\right) d\xi \, d\theta, \qquad i = 1 \ldots 4,$$

$$(NL)^{u}_{wn} = \frac{1}{2} \iint \begin{pmatrix} 2\alpha_{6n} \beta'_r \beta'_o \chi'_{\mathrm{i}} \psi_s \psi_p \vartheta_j + 2\alpha_{7n} \beta_r \beta_o \chi'_{\mathrm{i}} \psi'_s \psi'_p \vartheta_j \\ +\alpha_{8n} \beta'_r \beta_o \chi_i \psi_s \psi'_p \vartheta'_j + \alpha_{8n} \beta_r \beta'_o \chi_i \psi'_s \psi_p \vartheta'_j \end{pmatrix} d\xi \, d\theta,$$

$$(NL)_{wn}^{v}=\frac{1}{2}\iint\ \begin{pmatrix}2\alpha_{10n}\beta_r\beta_o\phi_k\psi_s'\psi_p'\alpha_l'+2\alpha_{11n}\beta_r'\beta_o'\phi_k\psi_s\psi_p\alpha_l'\\+\alpha_{14n}\beta_r'\beta_o\phi_k'\psi_s\psi_p'\alpha_l+\alpha_{14n}\beta_r\beta_o'\phi_k'\psi_s'\psi_p\alpha_l\end{pmatrix}d\xi\,d\theta,$$

$$(NL)_{w2n}^{w}=\frac{1}{2}\iint\ \begin{pmatrix}\alpha_{19n}\beta_r\beta_o'\beta_t'\psi_s\psi_p\psi_v+2\alpha_{19n}\beta_r'\beta_o'\beta_t\psi_s\psi_p\psi_v+\alpha_{20n}\beta_r\beta_o\beta_t\psi_s\psi_p'\psi_v'\\+2\alpha_{20n}\beta_r\beta_o\beta_t\psi_s'\psi_p'\psi_v-\bar{F}_{e3}(NL_{2e})_w^w\end{pmatrix}d\xi\,d\theta\,,$$

$$(NL_{2e})_{wn}^{w}=\beta_r\beta_o\beta_t\psi_s\psi_p\psi_v,$$

$$(NL)_{w3n}^{w}=\frac{1}{2}\iint\ \begin{pmatrix}4\alpha_{16n}\beta_r'\beta_o'\beta_t'\beta_a'\psi_s\psi_p\psi_v\psi_b+4\alpha_{17n}\beta_r\beta_o\beta_t\beta_a\psi_s'\psi_p'\psi_v'\psi_b'\\+2\alpha_{18n}\beta_r'\beta_o'\beta_t\beta_a\psi_s\psi_p\psi_v'\psi_b'+2\alpha_{18n}\beta_r\beta_o\beta_t'\beta_a'\psi_s'\psi_p'\psi_v\psi_b\\-\bar{F}_{e4}(NL_{3e})_w^w\end{pmatrix}d\xi\,d\theta$$

$$(NL_{3e})_{wn}^{w}=\beta_r\beta_o\beta_t\beta_a\psi_s\psi_p\psi_v\psi_b$$

$$(NL)_{win}^{vdw}=\frac{1}{2}\iint\ \left(\beta_r\beta_o\beta_t\beta_a\psi_s\psi_p\psi_v\psi_b\right)d\xi d\theta\,,\qquad i=1\dots4,$$

$$\bar{F}_{wp}=\frac{1}{2}\iint\ (\alpha_{25}\beta_r\psi_s+\alpha_{30}\beta_r''\psi_s+\alpha_{31}\beta_r\psi_s'')d\xi\,d\theta,\qquad \bar{F}_1=\iint\ (\beta_r\psi_s)d\xi\,d\theta\,,$$

$$\bar{F}_{e1}=\frac{1}{2}\bar{F}_e\bar{F}_1,\ \ \bar{F}_{eDC}=\frac{1}{2}\bar{F}_e\bar{V}_{DC}^2,\bar{F}_{we}=\bar{C}_1\bar{F}_{eDC}\bar{F}_1,\ \ \bar{F}_{e2}=\bar{C}_2\bar{F}_{eDC},\bar{F}_{e3}=\bar{C}_3\bar{F}_{eDC},\bar{F}_{e4}=\bar{C}_4\bar{F}_{eDC},$$

## Appendix 2

$$\alpha_{1n}=\frac{1}{m_{3n}}\bar{A}_{11n},\ \alpha_{2n}=\frac{m_{0n}^2}{m_{3n}}\bar{A}_{66n},\ \alpha_{3n}=\frac{m_{0n}}{m_{3n}}(\bar{A}_{12n}+\bar{A}_{21n}),\alpha_{4n}=\frac{2m_{0n}}{m_{3n}}\bar{A}_{66n},$$

$$\alpha_{5n}=\frac{m_{0n}}{m_{3n}}(\bar{A}_{12n}+\bar{A}_{21n}),\alpha_{6n}=\frac{1}{m_{1n}m_{3n}}\left(\bar{A}_{11n}-\bar{\tau}_{0n}^{ps}-\bar{\tau}_{0n}^{NI}\right),\ \alpha_{7n}=\frac{m_{0n}m_{2n}}{2m_{3n}}(\bar{A}_{12n}+\bar{A}_{21n}),$$

$$\alpha_{8n}=\frac{2m_{0n}m_{2n}}{m_{3n}}\bar{A}_{66n},\ \alpha_{9n}=\frac{m_{0n}^2}{m_{3n}}\bar{A}_{22n},\ \alpha_{10n}=\frac{m_{0n}^2m_{2n}}{m_{3n}}\left(\bar{A}_{22n}-\bar{\tau}_{0n}^{ps}-\bar{\tau}_{0n}^{NI}\right),$$

$$\alpha_{11n}=\frac{m_{2n}}{2m_{3n}}(\bar{A}_{12n}+\bar{A}_{21n}),\ \alpha_{12n}=\frac{2m_{0n}^2}{m_{3n}}\left(\bar{A}_{22n}-\bar{\tau}_{0n}^{ps}-\bar{\tau}_{0n}^{NI}\right),\alpha_{13n}=\frac{1}{m_{3n}}\bar{A}_{66n},$$

$$\alpha_{14n}=\frac{2m_{2n}}{m_{3n}}\bar{A}_{66n},\ \alpha_{15n}=\frac{m_{0n}^2}{m_{3n}}\left(\bar{A}_{22n}-2\left(\bar{\tau}_{0n}^{ps}+\bar{\tau}_{0n}^{NI}\right)\right),\ \alpha_{16n}$$

$$=\frac{1}{4m_{1n}^2m_{3n}}\left(\bar{A}_{11n}-2\left(\bar{\tau}_{0n}^{ps}+\bar{\tau}_{0n}^{NI}\right)\right),$$

$$\alpha_{17n}=\frac{m_{0n}^2m_{2n}^2}{4m_{3n}}\left(\bar{A}_{22n}-2\left(\bar{\tau}_{0n}^{ps}+\bar{\tau}_{0n}^{NI}\right)\right),\alpha_{18n}=\frac{m_{2n}^2}{4m_{3n}}(4\bar{A}_{66n}+\bar{A}_{12n}+\bar{A}_{21n}),$$

$$\alpha_{19n}=\frac{m_{2n}}{2m_{3n}}(\bar{A}_{12n}+\bar{A}_{21n}),\alpha_{20n}=\frac{m_{0n}^2m_{2n}}{m_{3n}}\left(\bar{A}_{22n}-2\left(\bar{\tau}_{0n}^{ps}+\bar{\tau}_{0n}^{NI}\right)\right),$$

$$\alpha_{21n}=\frac{1}{m_{1n}^2m_{3n}}(\bar{D}_{11n}-\bar{E}_{11n}),\ \alpha_{22n}=\frac{m_{0n}^2m_{2n}^2}{m_{3n}}(\bar{D}_{22n}-\bar{E}_{11n}),\ \alpha_{23n}=\frac{4m_{2n}^2}{m_{3n}}\bar{D}_{66n},$$

$$\alpha_{24n}=\frac{m_{2n}^2}{m_{3n}}(\bar{D}_{12n}+\bar{D}_{21n}-2\bar{E}_{11n}),\alpha_{25n}=\frac{m_{0n}m_{1n}}{m_{3n}}\left(2\left(\bar{\tau}_{0n}^{ps}+\bar{\tau}_{0n}^{NI}\right)-\bar{N}_{\theta pn}\right),$$

$$\alpha_{26n}=\frac{m_{1n}}{m_{3n}}\left(2\left(\bar{\tau}_{0n}^{ps}+\bar{\tau}_{0n}^{NI}\right)-\bar{N}_{xpn}\right),\alpha_{27n}=\frac{m_{0n}m_{1n}}{m_{3n}}\left(2\left(\bar{\tau}_{0n}^{ps}+\bar{\tau}_{0n}^{NI}\right)-\bar{N}_{\theta pn}\right),$$

$$\alpha_{28n}=\frac{1}{2m_{3n}}\left(2\left(\bar{\tau}_{0n}^{ps}+\bar{\tau}_{0n}^{NI}\right)-\bar{N}_{xpn}\right),\alpha_{29n}=\frac{m_{0n}^2}{2m_{3n}}\left(2\left(\bar{\tau}_{0n}^{ps}+\bar{\tau}_{0n}^{NI}\right)-\bar{N}_{\theta pn}\right),$$

$$\alpha_{30n}=\frac{1}{m_{3n}}\bar{M}_{xpn},\alpha_{31n}=\frac{m_{0n}^2}{m_{3n}}\bar{M}_{\theta pn},\alpha_{32n}=\frac{1}{2m_{1n}^2m_{3n}}\bar{G}_{11n}^*,\alpha_{33n}=\frac{m_{2n}^2}{2m_{3n}}\bar{G}_{11n}^*,$$

**References**


[1] Tichý, J.; Erhart, J.; Kittinger, E.; Prívratská, J. *Fundamentals of Piezoelectric Sensorics; Mechanical, Dielectric, and Thermodynamical Properties of Piezoelectric Materials*; Springer: U.S.A., 2010.

[2] Fang, X.Q.; Liu, J.X.; Gupta, V. *Nanoscale*. **2013**, 5, 1716.

[3] Tzou, H. *Piezoelectric Shells: Sensing, Energy Harvesting, and Distributed Control*; Springer: U.S.A., 2019.

[4] Gurtin, M.E.; Murdoch, A.I. *Int. J. Solids Struct*. **1978**, 14, 431–40.

[5] Strozzi, M.; Pellicano, F. *Math. Mech. Solids*. **2018**, 23, 1456-1481.

[6] Ghorbanpour Arani, A.; Kolahchi, R.; Khoddami Maraghi, Z. *Appl. Math. Modell*. **2013**, 37, 7685–7707.

[7] Malihi, S.; Tadi Beni, Y.; Golestanian, H. *Optik*. **2017,** 128, 156–171.

[8] Fakhrabadi, M. M. S.; Rastgoo, A.; Ahmadian, M.T. *Beilstein J. Nanotechnol*. **2013**, 4, 771-780.

[9] Fereidoon, A.; Andalib, E.; Mirafzal, A. Physica E. **2016,** 81, 205–218.

[10] Hashemi Kachapi, S.H.; Dardel, M.; Mohamadi daniali, H.; Fathi, A. *PI Mech. Eng. C J. Mech*. **2019**, DOI: 10.1177/0954406219845019.

[11] Hashemi Kachapi, S.H.; Dardel, M.; Mohamadi daniali, H.; Fathi, A. *Thin Walled Struct*. **2019**, 143, 106210.

[12] Hashemi Kachapi, S.H.; Dardel, M.; Mohamadi daniali, H.; Fathi, A. *Appl. Math. Modell*. **2019**, DOI:10.1016/j.apm.2019.05.035.

[13] Hashemi Kachapi, S.H.; Dardel, M.; Mohamadi daniali, H.; Fathi, A. *J. Vib. Control*, **2019**, DOI: 10.1177/1077546319889858.

[14] Fang, X.Q.; Zhu, C.S.; Liu, J.X.; Zhao, J. *Mater. Res. Express*. **2018**, 5.4, 045017.

[15] Wang, X. *Math. Mech. Solids*. **2018,** 23, 573-587.

[16] Nami, M. R.; Janghorban, M. *Beilstein J. Nanotechnol*. **2013**, 4, 968–973.

[17] Sigaeva, T.; Czekanski, A. *Math. Mech. Solids*. **2018**, 23, 715-726.

[18] Karimipour, I.; Tadi Beni, Y.; Zeighampour, H. *Microsyst. Technol*. **2017**, DOI 10.1007/s00542-017-3540-4.

[19] Farokhi, H. Nonlinear Behaviour of Carbon Nanotube Resonators with Applications in Mass-sensors. Ph. D. Thesis, McGill University, Canada, 2017.

[20] Rouhi, H.; Ansari, R.; Darvizeh, M. *J. Ultra. Graine. Nanostruct. Mat.* **2015,** 48, 113-124.

[21] Liu, Y.; Ji, X.; Wang, D.; He, J. *Eur. J. Mech. A. Solids*. **2019,** 74, 139-144.

[22] Jafari, S. B.; Malekfar, R.; Khadem, S. E. *int. J. Nanosci. Nanotechnol*. **2011,** 7, 137-142.

[23] He, X. Q.; Kitipornchai, S.; Liew, K. M. *J. Mech. Phys. Solids*. **2005,** 53, 303–326.

[24] Wang, L.; Ni, Q. A. *Mech. Res. Commun*. **2009**, 36, 833–837.